



1 **Title**

2 Decoupling of urban CO₂ and air pollutant emission reductions during the European
3 SARS-CoV2 lockdown

6
7 **Authors**

8 Christian Lamprecht¹, Martin Graus¹, Marcus Striednig¹, Michael Sticherer¹, and Thomas
9 Karl^{1*}

10
11
12
13 **Affiliations**

14 ¹ Institute for Atmospheric and Cryospheric Sciences, University of Innsbruck, Austria.

15
16
17 ***corresponding author, thomas.karl@uibk.ac.at**

18
19
20
21 **Abstract**

22
23 Lockdown and the associated massive reduction in people's mobility imposed by SARS-
24 CoV-2 mitigation measures across the globe provide a unique sensitivity experiment to
25 investigate impacts on carbon and air pollution emissions. We present an integrated observational
26 analysis based on long-term in-situ multispecies eddy flux measurements, allowing to quantify
27 near real time changes of urban surface emissions for key air quality and climate tracers. During
28 the first European SARS-CoV-2 wave we find that the emission reduction of classic air pollutants
29 decoupled from CO₂ and was significantly larger. These differences can only be rationalized by
30 the different nature of urban combustion sources, and point towards a systematic bias of
31 extrapolated urban NO_x emissions in state-of the art emission models. The analysis suggests that
32 European policies, shifting residential, public and commercial energy demand towards cleaner
33 combustion, have helped to improve air quality more than expected, and that the urban NO_x flux
34 remains to be dominated (e.g. >90%) by traffic.



42

43 **Introduction**

44

45

46

47

48

49

50

51

52

53

54

55

56

57

58

59

60

61

62

63

64

65

66

67

68

69

70

71

72

73

74

75

76

Managing air pollution and climate change are among the most important environmental challenges of modern society. As urban population continues to grow, emissions from metropolitan areas play an increasingly important role. For example, European cities already host about 74% of the population (UN, 2019) and are a major contributor to air pollutant and greenhouse gas emissions. Urban growth, along with socioeconomic development, and without mitigation can lead to substantial increases in anthropogenic emissions. Many cities are committing to sustainable development goals, and improvement of air pollution and mitigation of climate change are emerging as key sustainability priorities across the globe. Quantifying the diversity of urban emissions is often one of the most uncertain components of complex atmospheric models, and development of a robust predictive capability requires accurate data and careful evaluation of bottom-up emissions (Blain et al., 2019; NAS, 2016).

During the last two decades Europe's policy to reduce mid-term carbon emissions has fostered the proliferation of Diesel driven vehicles (EU-EUR-Lex, 2008). While soot emissions can be successfully removed with a Diesel particulate filter, the reduction of NO_x from Diesel exhaust has been more challenging, and was at the center of "Dieselgate" (Franco, V., Posada Sanches, F., German, J., Mock, 2014). As a consequence, European NO_x concentrations have declined less rapidly than elsewhere (Carslaw and Rhys-Tyler, 2013; Im et al., 2015; Karl et al., 2017), and put the EU-28 emission target for NO_x reductions (2005-2030: -63%) in jeopardy (EU-EUR-Lex, 2008). Nitrogen oxides have therefore emerged as a primary public health concern (Anenberg et al., 2017). European suppression measures due to the SARS-CoV2 outbreak provide a unique opportunity to track drastic changes in urban mobility during the lockdown phase, and combined with eddy flux methods allow investigating the sensitivity towards emission changes directly.

After the initial SARS—CoV2 emergence in China in late 2019, the World Health Organization declared the outbreak a global pandemic on March 11 2020. Worldwide measures to mitigate or suppress exponential growth of SARS-CoV2 have resulted in an unprecedented global intervention on mobility and industrial activity (WHO, 2020), allowing to study a number of environmental aspects (e.g. Liu et al., 2020b; Schiermeier, 2020; Quéré et al., 2020). A growing number of studies document regional and global air composition (e.g. Menut et al., 2020; Bao and Zhang, 2020) changes with respect to lockdown measures, including remote sensing observations and aspects of adequate data processing strategies (e.g. Liu et al., 2020a; Sussmann and Rettinger, 2020).



77 In Europe, most countries have implemented suppression strategies involving a more or
78 less extensive lockdown of public life. At the beginning of the pandemic, the level of suppression
79 varied among different countries, with some imposing very early ('China' like) lockdown
80 measures (e.g. Austria), others shifting from gradual social distancing measures to a lockdown
81 after re-consideration of alternative strategies (e.g. the UK). Depending on the magnitude of the
82 outbreak, European countries put increasingly stringent measures in place. The extent of different
83 lockdown measures has been assessed early on via cell phone activity tracking. For example,
84 Google mobility reports published in March 2020, suggested an 80% reduction of retail and
85 recreational activities across Europe. Traffic count data show a 60% reduction of urban mobility
86 due to a state-wide quarantine in the state of Tirol early during the pandemic. Such a drastic
87 mobility reduction during the suppression period allows performing a granular assessment of
88 processes impacting emissions and the distribution of air pollutant and climate gases. A direct and
89 quantitative way to assess air pollutant and climate gas emission changes can be based on the
90 eddy covariance method (Aubinet et al., 2012; Dabberdt et al., 1993). Briefly, in its simplest form
91 for stationary conditions and neglecting horizontal advection, the turbulent surface -atmosphere
92 flux (measured at height h) can represent the diffusive flux at the surface:

$$93 \quad \overline{(w'c')}_{h} = -D \left(\frac{\partial c}{\partial z} \right)_{0}, \quad (1)$$

94 where w' represents the vertical fluctuation of wind speed, D the molecular diffusion coefficient,
95 and c' the concentration fluctuation. The turbulent flux at the measurement height h (left side)
96 equals the diffusive surface flux (right side), which we are usually interested in. Brackets denote
97 the averaging interval. The ensemble average is typically 30 minutes. Eddy covariance
98 measurements have been extensively used in atmospheric sciences (Foken and Wichura, 1996;
99 Oncley et al., 2007; Patton et al., 2011) and biogeochemistry (Aubinet et al., 2012; Baldocchi et
100 al., 1988; Fowler et al., 2009; Rannik et al., 2012) (e.g. Ameriflux: <https://ameriflux.lbl.gov/>;
101 Euroflux: <http://www.europe-fluxdata.eu/icos>). The method has also become more tractable for
102 reactive trace gases such as NMVOC (Karl et al., 2001; Rinne et al., 2001; Spirig et al., 2005) or
103 NO_x (Lee et al., 2015), and has been used at urban sites (Christen, 2014; Langford et al., 2009;
104 Velasco et al., 2005). Urban eddy covariance methods can monitor aggregated emission changes
105 in real time. Here we build on a set of long-term multispecies flux and concentration datasets for
106 NO_x , O_3 , aromatic NMVOC, and CO_2 (Karl et al., 2020). Being inspired by early empirical
107 persistence models used in atmospheric chemistry and ecology, we propose a new quantitative
108 way for the analysis of urban fluxes during an intervention experiment by combining eddy
109 covariance data with a boosted regression tree model (Duffy and Helmbold, 2002). This method
110



111 allows to directly assess changes of surface fluxes for different trace gases in response to the
112 SARS-CoV2 lockdown and rebounding effects.
113
114



115 **Methods**

116

117 **IAO observations**

118

119 A site description of the Innsbruck Atmospheric Observatory (IAO), instrumentation and
120 site validation were previously described extensively (Karl et al., 2020). The flux footprint (Fig 1)
121 was calculated according to Kljun et al. (2015). For the measurement - inventory comparison we
122 mapped the two-dimensional climatological footprint (March-May) onto the spatially
123 disaggregated Austrian EMIKAT emission inventory (www.emikat.at). The relative seasonal
124 variability was accounted for by scaling total yearly traffic emissions to measured seasonal traffic
125 activity (Land Tirol, AT), and total yearly RCP emissions to measured seasonal NG consumption
126 (TIGAS, AT, <https://www.tigas.at/>). We assume that all fuel types used for heating appliances
127 and warm water consumption track relative changes of NG consumption, which is largely a
128 function of base load and degree heating days (Fig. S1). Traffic data were extracted from a
129 representative station near the flux tower provided by the Land Tirol. NO_x measurements were
130 based on a dual channel chemiluminescence instrument (CLD 899 Y; Ecophysics). The
131 instrument was operated in flux mode acquiring data at about 5Hz. A NO standard was
132 periodically introduced for calibration. Zeroing was performed once a day close to midnight. CO₂,
133 and H₂O were measured with a closed path eddy covariance system (CPEC 200; short inlet,
134 enclosed IRGA design; Campbell Scientific) along with three dimensional winds. Calibration for
135 CO₂ was performed once a day. Aromatic NMVOC (ie. benzene, toluene, xylenes+ethylbenzene,
136 and C₉ benzenes) were measured with a PTR-TOFMSx6000 mass spectrometer (IONICON, AT),
137 operated in hydronium mode at standard conditions in the drift tube of about 112 Townsend. The
138 instrument was set up to sample ambient air from a turbulently purged 3/8" Teflon line. Zero
139 calibrations were performed by providing NMVOC free air from a continuously purged
140 catalytical converter though a setup of software controlled solenoid valves. In addition, daily
141 calibrations were performed using known quantities of a suite of NMVOC from a 1ppm
142 calibration gas standard (Apel & Riemer, USA) that were added to the NMVOC free air and
143 dynamically diluted into low ppbv mixing ratios. This study builds on long-term NO_x and CO₂
144 flux measurements that run operationally since June 1st 2018. NMVOC fluxes were measured
145 during a field campaign from March 11th 2019 to April 9th 2019, and during the SARS-CoV2
146 lockdown, when measurements started on March 16th 2020. The NMVOC analysis presented in
147 this paper spans from March 16th 2020 to May 1st 2020.



148

149 **Boosted regression tree model**

150 Statistical persistence and regression models have a long history in atmospheric chemistry
151 (Robeson and Steyn, 1990) to predict empirical trends of pollutants (e.g. ozone), that factor in
152 meteorological and chemical processes. These approaches have been used to forecast local
153 surface ozone (Cobourn, 2007; Prybutok et al. 2000) and more recently trends of other
154 atmospheric pollutants (Grange and Carslaw, 2019). Here we developed a boosted regression tree
155 model using machine learning that is widely used in ecological modeling (Elith et al., 2008): for
156 each variable we based the model on the following key astronomical and environmental driving
157 variables: day of year (DOY), time of day (TOD), weekday/holiday (WDY), cartesian wind
158 vectors (NS- and WE-direction), temperature (T), relative humidity (RH), global radiation (GR)
159 and pressure (P). The model is setup using the machine learning toolbox in Matlab (Mathworks
160 Inc, USA) and trained for individual datasets until February 29th 2020 or during key reference
161 periods (SI Table S1). The model performance was assessed by comparing predicted and
162 observed quantities using reference datasets (SI Table S2). To obtain a quantitative measure of
163 emission changes, the differences between observed and predicted fluxes are integrated from the
164 beginning of the lockdown period. As the predicted and observed quantities diverge, the
165 integrated relative difference serves as a quantitative measure of emission (or activity) alteration
166 (e.g. reduction).

167

168 **Multispecies Pollutant Model**

169 Based on two major and distinct urban pollution sources (ie. road traffic and energy
170 production in the residential, public and commercial sectors) proportional contributions to the
171 observed flux changes can be attributed based on a two end member mixing model: Traffic
172 emissions are primarily related to exhaust from internal combustion engines. The Austrian
173 passenger car fleet is comprised of 43% gasoline and 55% Diesel driven cars (Statistik, Austria,
174 2020, www.statistik.at), with the latter being a key player for urban NO_x emissions. The second
175 significant emission source stems from fossil energy production in the residential, public and
176 commercial sectors with a significant contribution of natural gas combustion. In its simplest form
177 we can therefore aggregate the observed flux changes into two main emission source categories
178 using a two end member mixing model:

179

$$180 \frac{\delta F(s)}{F(s)} = a_s * \frac{\delta T}{T} + b_s * \frac{\delta R}{R} + \epsilon \quad (2),$$



181

182 where $\frac{\delta F(s)}{F(s)}$ is the measured relative flux difference between the boosted regression tree model
183 output and the actual flux observations of species s (e.g. NO_x , CO_2 , aromatic NMVOC), $\frac{\delta T}{T}$ is the
184 traffic load difference determined from traffic count data, $\frac{\delta R}{R}$ is the residential energy consumption
185 change, a_s and b_s are proportionality terms, and ε is an error term. The proportionality terms (a_s
186 and b_s) represent the area weighted emission factors of the fleet average traffic (a_s) and RCP
187 sector (b_s). By definition $a_s + b_s := 1$, if only two sources are considered.

188

189

190

191 Results

192

193 *The urban NO-NO₂-O₃ triad:* Due to the short atmospheric lifetime (e.g. up to 7 h
194 (Laughner and Cohen, 2019)) nitrogen oxides can serve as a gauge to assess air pollution changes
195 as their atmospheric concentrations rapidly respond to shifting surface fluxes. The quantitative
196 assessment of NO_x emissions based on ambient air concentrations however remains challenging
197 due to non-linearities within the $\text{NO-NO}_2\text{-O}_3$ triad in polluted regions (Lenschow et al., 2016).
198 Under sun-light conditions and high NO_x pollution the cycling between the $\text{NO-NO}_2\text{-O}_3$ triad is
199 described by the following reaction sequence:

200



204

205 The chemical timescale of the NO_x triad (eq 3 to 5) can be derived (Lenschow and Delany, 1987)
206 as

$$207 \quad \tau = \frac{2}{\sqrt{j^2 + k_3^2([\text{O}_3] - [\text{NO}])^2 + 2j \cdot k_3([\text{O}_3] + [\text{NO}] + 2 \cdot [\text{NO}_2])}} \quad (6)$$

208 For typical conditions encountered during this study, this equates to timescales of about
209 100 s, comparable to the vertical turbulent exchange time in cities. Due to the rapid
210 interconversion, the partitioning between NO and NO_2 is typically dominated by fast chemistry,
211 and the bulk of NO_2 in the urban atmosphere is produced secondarily via the reaction of NO and
212 O_3 . In the urban atmosphere this leads to a non-linear relationship between NO_2 and NO_x
213 concentrations as depicted in Fig. 2. A repartitioning can be observed during the suppression



214 phase for example, when the NO_2 to NO_x trajectory moves from an urban NO_x saturated regime to
215 a more NO_x limited regime. During the SARS-CoV2 lockdown this shift was more pronounced
216 than for typical weekend-weekday variations (Fig 2 B,C). As a consequence the relationship
217 between changes of NO_x fluxes and NO_2 concentrations becomes a non-linear function of NO_x
218 concentrations when moving from NO_x saturated to NO_x limited conditions. Data from a nearby
219 air quality station support these conclusions showing significantly different NO_x concentrations
220 during the 2020 lockdown compared to the previous 5 years (ie. a 50% reduction of NO_x), but no
221 significant change for O_x ($:= \text{NO}_2 + \text{O}_3$) based on the z hypothesis test. This chemical repartitioning
222 and vertical redistribution in the surface layer needs to be accounted for when quantifying
223 changing NO_x emissions from concentrations. A more quantitative picture of changing NO_x
224 emissions can be obtained from direct flux measurements that are intrinsically linked to surface
225 emissions (Vaughan et al., 2016).

226 Fig. 3 gives an overview of NO_x and CO_2 fluxes which have been continuously measured
227 at the study site in Central Europe since 2018. In addition, we have performed regular field
228 campaigns augmenting these long-term datasets with NMVOC flux measurements (Karl et al.,
229 2020). While atmospheric concentrations of primary air pollutants often exhibit strong surface
230 maxima due to inversion layers during winter and spring, the corresponding emission fluxes
231 typically track urban emission source activity and reflect changes in emission strengths and flux
232 footprint. Turbulent fluxes typically exhibit midday maxima, reflecting increases in urban
233 emission sources, which in the case of nitrogen oxides closely follow traffic load patterns (Karl et
234 al., 2017). Urban CO_2 fluxes follow these general trends, but are to some extent less pronounced
235 (e.g. weekend-weekday effect). During the vegetation period, CO_2 emission fluxes can be
236 suppressed (Ward et al., 2015) due to photosynthetic uptake by urban plants. For Innsbruck, we
237 have assessed this effect previously and find that within the flux footprint the contribution of
238 vegetation is relatively small (ie. only about 10% of the urban surface within the flux footprint is
239 covered by plants). Urban CO_2 fluxes are therefore primarily controlled by combustion processes.
240 The flux site is situated in a valley with two dominant wind sectors, which cover a typical inner
241 city residential and business district (Fig. 1) with no significant industrial activities. In order to
242 quantitatively investigate emission flux changes in response to SARS-CoV2 intervention
243 measures, we implemented a boosted regression tree model to define a business as usual scenario
244 of the observed fluxes (Duffy and Helmbold, 2002). The model allows factoring in differences in
245 weather patterns (e.g. meteorological variations such as temperature, wind direction and flux
246 footprint etc.), and describes changes that can be primarily attributed to the intervention itself.



247 Accounting for seasonal differences is key to an accurate analysis of emission alterations due to
248 lockdown measures. The essential time period of pre and post-lockdown measures in Europe
249 spans from March to about May 2020. Weather patterns in Europe can be particularly variable
250 during this period as the continent transitions from winter to summer. The climate of Tyrol is
251 fairly representative of central Europe, where the transitional period between March to May can
252 exhibit significant synoptic variability. For example, average monthly temperatures in March
253 2020 were about 0.9 K colder than in 2019. April and May 2020 tended to be 1.8 and 3.2 K
254 warmer than 2019. Warmer temperatures in spring 2020 resulted in 24% fewer degree heating
255 days (DHT) than in the year 2019 (SI). Consistent with these observations, natural gas
256 consumption in Tirol (SI) was reported to be 25% lower during this period than in 2019. We can
257 quantify changes of the observed fluxes due to the lockdown intervention in spring 2020 by
258 referencing actual flux measurements to results from a trained boosted regression tree model (Fig.
259 4).

260 Shortly after the European SARS-CoV2 outbreak first sparked in Italy, which was among
261 the first European countries, the greater part of the Alps was under lockdown by Mid-March to
262 inhibit cross-border transmission. Tyrol implemented extensive measures of shelter in place and a
263 state wide quarantine (QA) on top of the Austrian lockdown (LO) on March 16th, one week after
264 all Universities closed. At the same time, European wide measures of border control impacted all
265 major north-south transport corridors to Italy. These measures resulted in massively reduced local
266 mobility in combination with significant disruptions of one of the major transport routes across
267 the Alps. As a consequence, average traffic loads in Innsbruck decreased by ~60%. The Austrian
268 rate of infections reached a peak of 900 newly confirmed cases per day in Mid-March and started
269 to decline at the end of March. Along with efforts to reduce SARS-CoV2 transmission, the shelter
270 in place legislation resulted in a rapid decline of NO_x, CO₂ and aromatic NMVOC (benzene,
271 toluene, xylenes+ethylbenzene, and C₉ benzenes) fluxes (Fig. 4 A) reaching significantly lower
272 emission fluxes relative to the “business as usual” scenario. The cumulative reduction of surface
273 emissions of air pollutants (NO_x and aromatic NMVOC) closely follows traffic (Fig. 4 B and C),
274 declining by about 60% during the lock-down period. At the end of the Austrian Lockdown,
275 traffic counts and integrated emissions of NO_x, and aromatic NMVOC were -61 %, -59%, and -
276 56% lower compared to the business as usual scenario. This is significantly lower than the
277 observed reduction of CO₂ fluxes leveling out at about -38%. Notably benzene emissions also
278 declined less pronounced than toluene and higher aromatic NMVOC, which track NO_x and traffic
279 loads more closely. These different sensitivities indicate a non-linear relationship between the



280 reduction of carbon dioxide and air pollution gases due to different urban combustion sources.
281 Particularly reductions of NO_x and CO_2 exhibit quite different emission trajectories during the
282 lockdown phase (Fig. 5). The observed reduction of air pollution gases, such as NO_x , is
283 significantly larger than estimated by early bottom-up model predictions for expected NO_x to CO_2
284 emission changes (Quéré et al., 2020). Can these observations be reconciled with bottom-up
285 emission projections?

286

287 Discussion

288 Our analysis indicates that the reduction of classic air pollutant emissions during the
289 SARS-CoV2 lockdown was more significant than that of CO_2 which comes as surprise.
290 Comparable to most European countries, Austrian specific bottom up emission models typically
291 attribute 40% of CO_2 emissions to traffic and 19% to the residential, commercial and public
292 (RCP) sector (UBA, 2019). For NO_x , Austrian and European bottom-up emission projections
293 predict similar contributions (ie. 58% from traffic and 12% from the RCP sector). In its simplest
294 form, by using a two member pollutant model, we can test these assumptions in more detail, and
295 compare our observations with an Austrian state of the art emission model (www.emikat.at) used
296 for national emission reporting. For the analysis we take advantage of the fact that the seasonal
297 influence on pollutant fluxes is factored in by referencing the flux analysis to the trained boosted
298 regression tree model. Further, measured relative reductions of vehicle counts are assumed to
299 represent the decrease of traffic activity reasonably well. We are then left with constraining the
300 intervention specific changes in the RCP sector. We argue that these must not have changed
301 much, because (a) heating appliances are primarily driven by temperature (Liu et al., 2020b)
302 (accounted for by our analysis) (b) changes in electricity needs do not enter the local pollutant
303 budget, and (c) less time spent in commercial/public buildings was compensated by more time in
304 residential buildings. Google mobility reports (Alphabet Inc., 2020) based on cellphone tracking
305 suggest a 20% increase in time spent in the residential sector and a 30% decrease in the
306 commercial/public sector for Tyrol during the lockdown period. Liu et al. (2020) estimated a
307 decline of commercial and residential emissions by 3.6%, Le Quéré et al. (2020) assumed an
308 increase of residential emissions by 4% and a decrease in the public sector by 33% for Europe. As
309 a conservative estimate we bracket changes in the RCP sector activity between 0 and -20%, with
310 a best estimate based on the local Google mobility index (-10%). The observed flux changes can
311 then be partitioned into NO_x emissions from vehicular traffic ($98_{-11}^{+2}\%$) and the RCP sector
312 ($2_{-2}^{+11}\%$) accordingly. For CO_2 , benzene, toluene and the sum of aromatic NMVOC we calculate
313 $55_{-10}^{+7}\%$, $69_{-7}^{+5}\%$, $98_{-11}^{+2}\%$, and $90_{-11}^{+2}\%$ arising from vehicular traffic emissions, and $45_{-11}^{+7}\%$,



314 $31^{+5}_{-8}\%$, $2^{+11}_{-1}\%$, and $10^{+2}_{-3}\%$ respectively, coming from the RCP sector. These results suggest that
315 NO_x is dominated by vehicular traffic emissions and that CO_2 is partitioned more equally between
316 the traffic and RCP sectors. In contrast, urban NMVOC emissions are generally more diverse
317 (Karl et al., 2018). Here we investigate aromatic NMVOC, that are closely linked to combustion
318 processes and fossil fuel use (EPA, 1998). We observe that toluene and higher aromatic NMVOCs
319 closely track reductions of NO_x emissions and vehicular traffic activity. Benzene declined less
320 readily, suggesting that benzene emissions could be more prevalent from the RCP sector.
321 Speciated NMVOC emission factors from residential gas and oil combustion are still quite
322 uncertain, but recent reports from shale gas operations in the US for example indicate a higher
323 contribution of benzene than toluene emissions from natural gas combustion when compared to
324 traffic sources (Gilman et al., 2013; Halliday et al., 2016; Helmig et al., 2014).

325 After mapping NO_x and CO_2 emissions from a spatially disaggregated emission model on
326 the seasonal flux footprint (SI), the observationally inferred results from above can be compared
327 to the relative attribution of inventory based emission projections. As for NO_x and CO_2 , the
328 official local bottom up emission inventory apportions 78% of NO_x fluxes coming from vehicular
329 traffic, and 21% from the RCP sector. For CO_2 these relative contributions are 54% (traffic
330 sector) and 46% (RCP sector), respectively. These inventory based results are roughly in line with
331 a recently published bottom-up assessment for CO_2 emissions (Quéré et al., 2020). We also find
332 that CO_2 fluxes are consistent with the relative emission attribution in the inventory, but that NO_x
333 emissions are significantly overestimated from the RCP sector (e.g. 21% vs 2%) in favor of traffic
334 (Fig. 4). This suggests cleaner NO_x combustion sources in the RCP sector and higher NO_x
335 emissions from the traffic sector.

336 The European gas demand has increased significantly over the past decades (European
337 Commission, n.d.). As an example, consumption of natural gas increased by about a factor of 4 in
338 Austria (Statistik Austria, 2019) since 1965, and has expanded to 9 billion m^3 . Across Europe
339 growing demand has increased dependence on gas imports, triggering fierce competition between
340 major gas producing nations (European Commission, n.d.). Apart from the power sector,
341 residential demand has contributed significantly to the overall consumption growth across
342 Europe (European Commission, n.d.). While residential gas consumption per inhabitant varies
343 quite drastically across European countries, many countries have invested in developing the
344 residential sector towards a higher fraction of natural gas by fuel subsidy policies. Particularly
345 urban areas, where gas infrastructure is in place, have seen significant growth. As an example, the
346 residential energy sector has seen a doubling of the natural gas share for space heating appliances



347 in Western Austria over the last 9 years (Statistik Austria, 2019). In parallel, oil and solid fuel
348 consumption have decreased by about 40% in the residential sector over the same period. On
349 average, gas represents about a third of the final energy consumption in the residential sector in
350 Austria and across Europe (European Commission, 2018). One of the reasons for promoting
351 natural gas through subsidies in the past was that gas combustion releases about 25% less CO₂
352 than oil and 40% less than solid fuels (IEA, 2020). In addition to more efficient energy
353 production, natural gas combustion releases less air toxics, such as NO_x, CO, NMVOC and SO₂,
354 when compared to biomass and other solid fuels (EEA, 2019). However, emissions from the RCP
355 sector are quite uncertain and often rely on TIER I upscaling methodology (Blain et al., 2019;
356 EEA, 2019). As the European community is committed to transitioning to a carbon-neutral
357 economy (OECD, 2015), the air quality benefit from natural gas in the residential sector needs to
358 be considered, particularly when introducing renewable alternatives such as wood and pellet
359 combustion on a large scale. Our data suggest that the air quality benefit for the release of reactive
360 nitrogen in the RCP sector might have been underestimated in bottom-up emission inventories
361 used for policy making. Official inventory data show that the increase of natural gas combustion
362 in the RCP played a significant role in Europe's energy policy. Wood combustion on the other
363 hand would release significant amounts of reactive nitrogen in the gas and aerosol phase
364 depending on fuel N content (Roberts et al., 2020). While pellet combustion is considered cleaner
365 than wood combustion, TIER I emission factors for NO_x are still about twice as high compared to
366 natural gas combustion, and the release of aerosols is of particular concern (EEA, 2019). When
367 transitioning to a climate neutral economy, the air quality penalty arising from some renewables
368 needs to be sustainable. From the present analysis we find that the biggest gain for the reduction
369 of urban NO_x in Europe remains in the mobility sector, and that NO_x emissions from the RCP
370 sector are significantly lower than expected. Europe's push towards a Diesel driven car fleet has
371 helped to curb CO₂ emissions in the mobility sector, but created excess emissions of nitrogen
372 oxides. While the extent of cheating devices used in cars to simulate lower than actual NO_x
373 emissions is still unravelling, aggressive reductions of nitrogen oxides are needed to meet
374 Europe's air quality goals (EU-EUR-Lex, 2008). A significant NO_x emission reduction in the
375 mobility sector could help counteract potential increases of air pollutants from promoted
376 renewables such as biomass combustion in the future. Urban eddy flux methods present a top
377 down methodology allowing to quantify and test urban sustainability goals of air pollution and
378 climate gas emissions. In combination with an intervention experiment as shown here they can



379 provide a unique and independent verification method of anticipated air quality and climate policy
380 targets.

381 **References**

- 382
383 Alphabet Inc.: Google LLC Community Mobility Reports, 2020 [online] Available from:
384 <https://www.google.com/covid19/mobility/>, 2020.
- 385 Anenberg, S. C., Miller, J., Minjares, R., Du, L., Henze, D. K., Lacey, F., Malley, C. S.,
386 Emberson, L., Franco, V., Klimont, Z. and Heyes, C.: Impacts and mitigation of excess diesel-
387 related NO_x emissions in 11 major vehicle markets, *Nature*, 545(7655), 467–471,
388 doi:10.1038/nature22086, 2017.
- 389 Aubinet, M., Vesala, T. and Papale, D.: Eddy Covariance: A Practical Guide to Measurement and
390 Data Analysis, Springer. [online] Available from: <https://doi.org/10.1007/978-94-007-2351-1>,
391 2012.
- 392 Baldocchi, D. D., Hincks, B. B. and Meyers, T. P.: Measuring Biosphere-Atmosphere Exchanges
393 of Biologically Related Gases with Micrometeorological Methods, *Ecology*, 69(5), 1331–1340,
394 doi:10.2307/1941631, 1988.
- 395 Bao, R. and Zhang, A.: Does lockdown reduce air pollution? Evidence from 44 cities in northern
396 China, *Sci. Total Environ.*, 731, 139052, doi:10.1016/j.scitotenv.2020.139052, 2020.
- 397 Blain, W., Buendia, C., Fuglestedt, E. and Al., E.: Short lived climate forcers, edited by W.
398 Blain, D., Calvo Buendia, E., Fuglestedt, J.S., Gómez, D., Masson-Delmotte, V., Tanabe, K.,
399 Yassaa, N., Zhai, P., Kranjc, A., Jamsranjav, B., Ngarize, S., Pyrozhenko, Y., Shermanau, P.,
400 Connors, S., Moufouma-Okia, pp. 1–66, Institute for Global Environmental Strategies. [online]
401 Available from:
402 https://www.ipcc.ch/site/assets/uploads/2019/02/1805_Expert_Meeting_on_SLCF_Report.pdf,
403 2019.
- 404 Carslaw, D. C. and Rhys-Tyler, G.: New insights from comprehensive on-road measurements of
405 NO_x, NO₂ and NH₃ from vehicle emission remote sensing in London, UK, *Atmos. Environ.*, 81,
406 339–347, doi:10.1016/j.atmosenv.2013.09.026, 2013.
- 407 Christen, A.: Atmospheric measurement techniques to quantify greenhouse gas emissions from
408 cities, *Urban Clim.*, 10, 241–260, doi:10.1016/j.uclim.2014.04.006, 2014.
- 409 Cobourn, W. G.: Accuracy and reliability of an automated air quality forecast system for ozone in
410 seven Kentucky metropolitan areas, *Atmos. Environ.*, 41(28), 5863–5875,
411 doi:10.1016/j.atmosenv.2007.03.024, 2007.
- 412 Dabberdt, W. F., Lenschow, D. H., Horst, T. W., Zimmerman, P. R., Oncley, S. P. and Delany, A.
413 C.: Atmosphere-Surface Exchange Measurements, *Science*, 260(5113), 1472–1481,
414 doi:10.1126/science.260.5113.1472, 1993.
- 415 Duffy, N. and Helmbold, D.: Boosting Methods for Regression, *Mach. Learn.*, 47(2/3), 153–200,
416 doi:10.1023/a:1013685603443, 2002.
- 417 EEA: EMEP/EEA air pollutant emission inventory guidebook. [online] Available from:
418 [https://www.eea.europa.eu/themes/air/air-pollution-sources-1/emep-eea-air-pollutant-emission-](https://www.eea.europa.eu/themes/air/air-pollution-sources-1/emep-eea-air-pollutant-emission-inventory-guidebook/emep)
419 [inventory-guidebook/emep](https://www.eea.europa.eu/themes/air/air-pollution-sources-1/emep-eea-air-pollutant-emission-inventory-guidebook/emep), 2019.
- 420 Elith, J., Leathwick, J. R. and Hastie, T.: A working guide to boosted regression trees, *J. Anim.*
421 *Ecol.*, 77(4), 802–813, doi:10.1111/j.1365-2656.2008.01390.x, 2008.
- 422 EPA: Locating and estimating air emissions from sources of benzene., 1998.
- 423 EU-EUR-Lex: Directives 1999/94/EC and 2008/50/EC. [online] Available from: [https://eur-](https://eur-lex.europa.eu/legal-content/EN/TXT/?uri=CELEX%3A31999L0094)
424 [lex.europa.eu/legal-content/EN/TXT/?uri=CELEX%3A31999L0094](https://eur-lex.europa.eu/legal-content/EN/TXT/?uri=CELEX%3A31999L0094), n.d.
- 425 European Commission: Gas and electricity market reports. [online] Available from:
426 https://ec.europa.eu/energy/data-analysis/market-analysis_en, n.d.
- 427 Foken, T. and Wichura, B.: Tools for quality assessment of surface-based flux measurements,



- 428 Agric. For. Meteorol., 78(1–2), 83–105, doi:10.1016/0168-1923(95)02248-1, 1996.
- 429 Fowler, D., Pilegaard, K., Sutton, M. A., Ambus, P., Raivonen, M., Duyzer, J., Simpson, D.,
430 Fagerli, H., Fuzzi, S., Schjoerring, J. K., Granier, C., Neftel, A., Isaksen, I. S. A., Laj, P., Maione,
431 M., Monks, P. S., Burkhardt, J., Daemmgen, U., Neiryneck, J., Personne, E., Wichink-Kruit, R.,
432 Butterbach-Bahl, K., Flechard, C., Tuovinen, J. P., Coyle, M., Gerosa, G., Loubet, B., Altimir, N.,
433 Gruenhage, L., Ammann, C., Cieslik, S., Paoletti, E., Mikkelsen, T. N., Ro-Poulsen, H., Cellier,
434 P., Cape, J. N., Horváth, L., Loreto, F., Niinemets, U., Palmer, P. I., Rinne, J., Misztal, P.,
435 Nemitz, E., Nilsson, D., Pryor, S., Gallagher, M. W., Vesala, T., Skiba, U., Brüggemann, N.,
436 Zechmeister-Boltenstern, S., Williams, J., O'Dowd, C., Facchini, M. C., de Leeuw, G., Flossman,
437 A., Chaumerliac, N. and Erisman, J. W.: Atmospheric composition change: Ecosystems
438 Atmosphere interactions, *Atmos. Environ.*, 43(33), 5193–5267,
439 doi:10.1016/j.atmosenv.2009.07.068, 2009.
- 440 Franco, V., Posada Sanches, F., German, J., Mock, P.: Real-world exhaust emissions from
441 modern diesel cars, ICCT, 1–52 [online] Available from: www.icct.org, 2014.
- 442 Gilman, J. B., Lerner, B. M., Kuster, W. C. and de Gouw, J. A.: Source Signature of Volatile
443 Organic Compounds from Oil and Natural Gas Operations in Northeastern Colorado, *Environ.*
444 *Sci. Technol.*, 47(3), 1297–1305, doi:10.1021/es304119a, 2013.
- 445 Grange, S. K. and Carslaw, D. C.: Using meteorological normalisation to detect interventions in
446 air quality time series, *Sci. Total Environ.*, 653, 578–588, doi:10.1016/j.scitotenv.2018.10.344,
447 2019.
- 448 Halliday, H. S., Thompson, A. M., Wisthaler, A., Blake, D. R., Hornbrook, R. S., Mikoviny, T.,
449 Müller, M., Eichler, P., Apel, E. C. and Hills, A. J.: Atmospheric benzene observations from oil
450 and gas production in the Denver-Julesburg Basin in July and August 2014, *J. Geophys. Res.*
451 *Atmos.*, 121(18), 1111–5574, doi:10.1002/2016jd025327, 2016.
- 452 Helmig, D., Thompson, C. R., Evans, J., Boylan, P., Hueber, J. and Park, J.-H.: Highly Elevated
453 Atmospheric Levels of Volatile Organic Compounds in the Uintah Basin, Utah, *Environ. Sci.*
454 *Technol.*, 48(9), 4707–4715, doi:10.1021/es405046r, 2014.
- 455 IEA: Fuels and technologies. [online] Available from: [https://www.iea.org/fuels-and-](https://www.iea.org/fuels-and-technologies%0D%0A)
456 [technologies%0D%0A](https://www.iea.org/fuels-and-technologies%0D%0A), 2020.
- 457 Im, U., Bianconi, R., Solazzo, E., Kioutsioukis, I., Badia, A., Balzarini, A., Baro, R., Bellasio, R.,
458 Brunner, D., Chemel, C., Curci, G., Flemming, J., Forkel, R., Giordano, L., Jimenez-Guerrero, P.,
459 Hirtl, M., Hodzic, A., Honzak, L., Jorba, O., Knote, C., Kuenen, J. J. P., Makar, P. A., Manders-
460 Groot, A., Neal, L., Perez, J. L., Pirovano, G., Pouliot, G., San Jose, R., Savage, N., Schroder, W.,
461 Sokhi, R. S., Syrakov, D., Torian, A., Tuccella, P., Werhahn, J., Wolke, R., Yahya, K., Zabkar,
462 R., Zhang, Y., Zhang, J., Hogrefe, C. and Galmarini, S.: Evaluation of operational on-line-
463 coupled regional air quality models over Europe and North America in the context of AQMEII
464 phase 2. Part I: Ozone, *Atmos. Environ.*, 115, 404–420, doi:10.1016/j.atmosenv.2014.09.042,
465 2015.
- 466 Karl, T., Guenther, A., Jordan, A., Fall, R. and Lindinger, W.: Eddy covariance measurement of
467 biogenic oxygenated VOC emissions from hay harvesting, *Atmos. Environ.*, 35(3), 491–195,
468 doi:10.1016/S1352-2310(00)00405-2, 2001.
- 469 Karl, T., Graus, M., Striednig, M., Lamprecht, C., Hammerle, A., Wohlfahrt, G., Held, A., Von
470 Der Heyden, L., Deventer, M. J., Krismer, A., Haun, C., Feichter, R. and Lee, J.: Urban eddy
471 covariance measurements reveal significant missing NO_x emissions in Central Europe, *Sci. Rep.*,
472 7(1), 1–9, doi:10.1038/s41598-017-02699-9, 2017.
- 473 Karl, T., Striednig, M., Graus, M., Hammerle, A. and Wohlfahrt, G.: Urban flux measurements
474 reveal a large pool of oxygenated volatile organic compound emissions, *Proc. Natl. Acad. Sci.*,
475 115(6), 1186–1191, doi:10.1073/pnas.1714715115, 2018.
- 476 Karl, T., Gohm, A., Rotach, M., Ward, H., Graus, M., Cede, A., Wohlfahrt, G., Hammerle, A.,
477 Haid, M., Tiefengraber, M., Lamprecht, C., Vergeiner, J., Kreuter, A., Wagner, J. and Staudinger,



- 478 M.: Studying Urban Climate and Air quality in the Alps - The Innsbruck Atmospheric
479 Observatory, *Bull. Am. Meteorol. Soc.*, in press, 2020.
- 480 Kljun, N., Calanca, P., Rotach, M. W. and Schmid, H. P.: A simple two-dimensional
481 parameterisation for Flux Footprint Prediction (FFP), *Geosci. Model Dev.*, 8(11), 3695–3713,
482 doi:10.5194/gmd-8-3695-2015, 2015.
- 483 Langford, B., Davison, B., Nemitz, E. and Hewitt, C. N.: Mixing ratios and eddy covariance flux
484 measurements of volatile organic compounds from an urban canopy (Manchester, UK), *Atmos.*
485 *Chem. Phys.*, 9(6), 1971–1987, doi:10.5194/acp-9-1971-2009, 2009.
- 486 Laughner, J. L. and Cohen, R. C.: Direct observation of changing NO_x lifetime in North
487 American cities, *Science*, 366(6466), 723–727, doi:10.1126/science.aax6832, 2019.
- 488 Lee, J. D., Helfter, C., Purvis, R. M., Beevers, S. D., Carslaw, D. C., Lewis, A. C., Moller, S. J.,
489 Tremper, A., Vaughan, A. and Nemitz, E. G.: Measurement of NO_x Fluxes from a Tall Tower in
490 Central London, UK and Comparison with Emissions Inventories, *Environ. Sci. Technol.*, 49(2),
491 1025–1034, doi:10.1021/es5049072, 2015.
- 492 Lenschow, D. H. and Delany, A. C.: An analytic formulation for NO and NO₂ flux profiles in the
493 atmospheric surface layer, *J. Atmos. Chem.*, 5(3), 301–309, doi:10.1007/bf00114108, 1987.
- 494 Lenschow, D. H., Gurarie, D. and Patton, E. G.: Modeling the diurnal cycle of conserved and
495 reactive species in the convective boundary layer using SOMCRUS, *Geosci. Model Dev.*, 9(3),
496 979–996, doi:10.5194/gmd-9-979-2016, 2016.
- 497 Liu, F., Page, A., Strode, S. A., Yoshida, Y., Choi, S., Zheng, B., Lamsal, L. N., Li, C., Krotkov,
498 N. A., Eskes, H., van der A, R., Veefkind, P., Levelt, P. F., Hauser, O. P. and Joiner, J.: Abrupt
499 decline in tropospheric nitrogen dioxide over China after the outbreak of COVID-19, *Sci. Adv.*,
500 6(28), 1–5, doi:10.1126/sciadv.abc2992, 2020a.
- 501 Liu, Z., Ciais, P., Deng, Z. and Al., E.: COVID-19 causes record decline in global CO₂
502 emissions, arXiv, 1–45 [online] Available from: <http://arxiv.org/abs/2004.13614>, 2020b.
- 503 Menut, L., Bessagnet, B., Siour, G., Mailler, S., Pennel, R. and Cholakian, A.: Impact of
504 lockdown measures to combat Covid-19 on air quality over western Europe, *Sci. Total Environ.*,
505 741, 140426, doi:10.1016/j.scitotenv.2020.140426, 2020.
- 506 NAS, U.: *The Future of Atmospheric Chemistry Research: Remembering Yesterday,*
507 *Understanding Today, Anticipating Tomorrow*, The National Academies Press, Washington, DC.,
508 2016.
- 509 OECD: *Aligning Policies for a Low-carbon Economy*, OECD., 2015.
- 510 Oncley, S. P., Foken, T., Vogt, R., Kohsiek, W., DeBruin, H. A. R., Bernhofer, C., Christen, A.,
511 van Gorsel, E., Grantz, D., Feigenwinter, C., Lehner, I., Liebenthal, C., Liu, H., Mauder, M.,
512 Pitacco, A., Ribeiro, L. and Weidinger, T.: The Energy Balance Experiment EBEX-2000. Part I:
513 overview and energy balance, *Boundary-Layer Meteorol.*, 123(1), 1–28, doi:10.1007/s10546-007-
514 9161-1, 2007.
- 515 Patton, E. G., Horst, T. W., Sullivan, P. P., Lenschow, D. H., Oncley, S. P., Brown, W. O. J.,
516 Burns, S. P. P., Guenther, A. B., Held, A., Karl, T., Mayor, S. D., Rizzo, L. V., Spuler, S. M.,
517 Sun, J., Turnipseed, A. A., Awine, E. J., Edburg, S. L., Lamb, B. K., Avissar, R., Calhoun, R. J.,
518 Kleissl, J., Massman, W. J., Paw U, K. T. and Weil, J. C.: The canopy horizontal array turbulence
519 study, *Bull. Am. Meteorol. Soc.*, 92(5), 593–611, doi:10.1175/2010BAMS2614.1, 2011.
- 520 Prybutok, V. R., Yi, J. and Mitchell, D.: Comparison of neural network models with ARIMA and
521 regression models for prediction of Houstons daily maximum ozone concentrations, *Eur. J. Oper.*
522 *Res.*, 122(1), 31–40, doi:10.1016/s0377-2217(99)00069-7, 2000.
- 523 Quéré, C. Le, Jackson, R. B., Jones, M. W., Smith, A. J. P., Abernethy, S., Andrew, R. M., De-
524 Gol, A. J., Willis, D. R., Shan, Y., Canadell, J. G., Friedlingstein, P., Creutzig, F. and Peters, G.
525 P.: Temporary reduction in daily global CO₂ emissions during the COVID-19 forced
526 confinement, *Nat. Clim. Chang.*, 10(7), 647–653, doi:10.1038/s41558-020-0797-x, 2020.
- 527 Rannik, U., Altimir, N., Mammarella, I., Baeck, J., Rinne, J., Ruuskanen, T. M., Hari, P., Vesala,



- 528 T. and Kulmala, M.: Ozone deposition into a boreal forest over a decade of observations:
529 evaluating partitioning and driving variables, *Atmos. Chem. Phys.*, 12(24), 12165–
530 12182, doi:10.5194/acp-12-12165-2012, 2012.
- 531 Rinne, H. J. I., Guenther, A. B., Warneke, C., de Gouw, J. A. and Luxembourg, S. L.: Disjunct
532 eddy covariance technique for trace gas flux measurements, *Geophys. Res. Lett.*, 28(16), 3139–
533 3142, doi:10.1029/2001gl012900, 2001.
- 534 Roberts, J. M., Stockwell, C. E., Yokelson, R. J., de Gouw, J., Liu, Y., Selimovic, V., Koss, A. R.,
535 Sekimoto, K., Coggon, M. M., Yuan, B., Zarzana, K. J., Brown, S. S., Santin, C., Doerr, S. H. and
536 Warneke, C.: The nitrogen budget of laboratory-simulated western US wildfires during the
537 FIREX 2016 Fire Lab study, *Atmos. Chem. Phys.*, 20(14), 8807–8826, doi:10.5194/acp-20-8807-
538 2020, 2020.
- 539 Robeson, S. M. and Steyn, D. G.: Evaluation and comparison of statistical forecast models for
540 daily maximum ozone concentrations, *Atmos. Environ. Part B. Urban Atmos.*, 24(2), 303–312,
541 doi:10.1016/0957-1272(90)90036-t, 1990.
- 542 Schiermeier, Q.: Why pollution is plummeting in some cities, but not others, *Nature*, 580(7803),
543 313, doi:10.1038/d41586-020-01049-6, 2020.
- 544 Spirig, C., Neftel, A., Ammann, C., Dommen, J., Grabmer, W., Thielmann, A., Schaub, A.,
545 Beauchamp, J., Wisthaler, A. and Hansel, A.: Eddy covariance flux measurements of biogenic
546 VOCs during ECHO 2003 using proton transfer reaction mass spectrometry, *Atmos. Chem. Phys.*,
547 5, 465–481, doi:10.5194/acp-5-465-2005, 2005.
- 548 Statistik Austria: Energiebilanzen, [online] Available from:
549 [https://www.statistik.at/web_de/statistiken/energie_umwelt_innovation_mobilitaet/energie_und_u](https://www.statistik.at/web_de/statistiken/energie_umwelt_innovation_mobilitaet/energie_und_umwelt/energie/energiebilanzen/index.html)
550 [mwelt/energie/energiebilanzen/index.html](https://www.statistik.at/web_de/statistiken/energie_umwelt_innovation_mobilitaet/energie_und_umwelt/energie/energiebilanzen/index.html), 2019.
- 551 Sussmann, R. and Rettinger, M.: Can We Measure a COVID-19-Related Slowdown in
552 Atmospheric CO₂ Growth? Sensitivity of Total Carbon Column Observations, *Remote Sens.*, 12,
553 1–22, doi:10.3390/rs12152387, 2020.
- 554 UBA: Bundeslaender Luftschadstoffinventur 1990-2017. [online] Available from:
555 <https://www.umweltbundesamt.at/fileadmin/site/publikationen/rep0703.pdf>, 2019.
- 556 UN: World Population Prospects 2019, Volume II: Demographic Profiles. [online] Available
557 from: <https://population.un.org/wpp/Publications/>, 2019.
- 558 Vaughan, A. R., Lee, J. D., Misztal, P. K., Metzger, S., Shaw, M. D., Lewis, A. C., Purvis, R. M.,
559 Carslaw, D. C., Goldstein, A. H., Hewitt, C. N., Davison, B., Beevers, S. D. and Karl, T. G.:
560 Spatially resolved flux measurements of NO_x from London suggest significantly higher
561 emissions than predicted by inventories, *Faraday Discuss.*, 189, doi:10.1039/c5fd00170f, 2016.
- 562 Velasco, E., Lamb, B., Presseley, S. and Al., E.: Flux measurements of volatile organic
563 compounds from an urban landscape, *Geophys. Res. Lett.*, 32(20), 1–4,
564 doi:10.1029/2005gl023356, 2005.
- 565 Ward, H. C., Kotthaus, S., Grimmond, C. S. B., Borgeggen, A., Wilkinson, M., Morrison, W. T.
566 J., Evans, J. G., Morison, J. I. L. and Iamarino, M.: Effects of urban density on carbon dioxide
567 exchanges: Observations of dense urban, suburban and woodland areas of southern England,
568 *Environ. Pollut.*, 198, 186–200, doi:10.1016/j.envpol.2014.12.031, 2015.
- 569 WHO: Report of the WHO-China Joint Mission on Coronavirus Disease 2019 (COVID-19).
570 [online] Available from: [https://www.who.int/publications-detail/report-of-the-who-china-joint-](https://www.who.int/publications-detail/report-of-the-who-china-joint-mission-on-coronavirus-disease-2019-(covid-19))
571 [mission-on-coronavirus-disease-2019-\(covid-19\)](https://www.who.int/publications-detail/report-of-the-who-china-joint-mission-on-coronavirus-disease-2019-(covid-19)), 2020.

572

573

574 Acknowledgments

575

576 We thank Christoph Haun, Land Tirol, Johann Haun, TIGAS, and Florian Haidacher,
577 Land Tirol, for providing official emissions, gas consumption and traffic data referenced

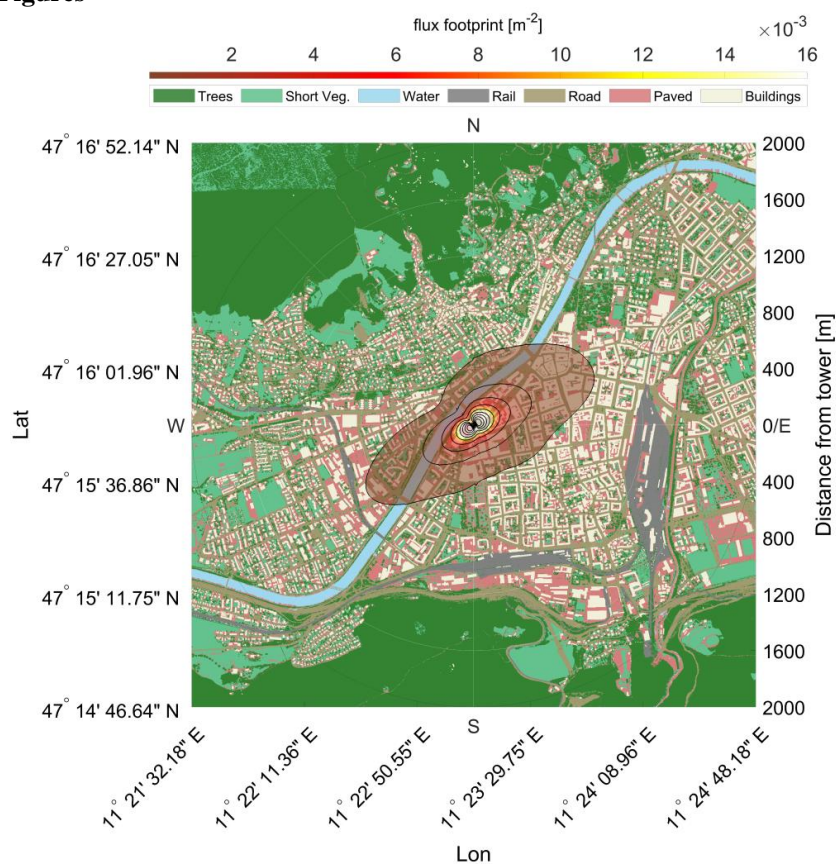


578 in this study. Funding: This work was supported by the Austrian National Science fund
579 (FWF) through grant P30600. Author contributions: T.K. conceived the overall analysis.
580 T.K., C.L., M.G. designed and performed the field experiments, and interpreted the data.
581 M.S. (1) conducted the NMVOC flux analysis. M.S. (2) assisted with the field
582 experiments. All authors contributed to writing the manuscript.

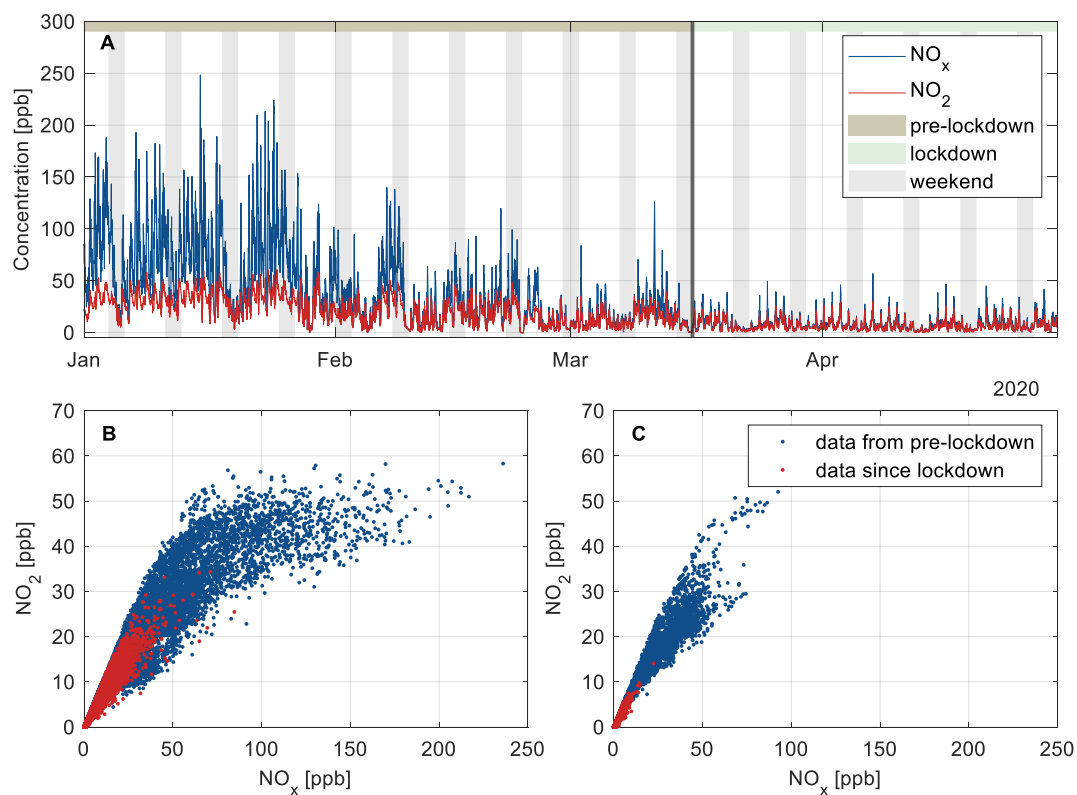
583
584
585



586
587 **Figures**

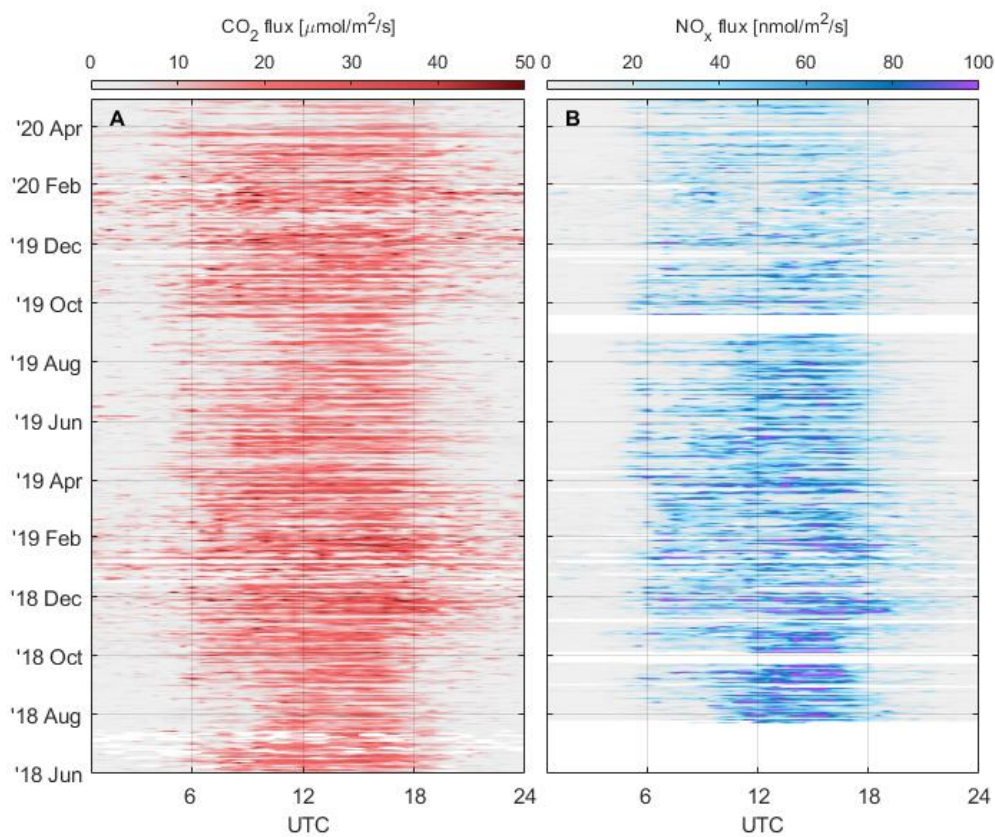


588
589
590 **Fig. 1:** Flux footprint surrounding the IAO tower plotted on top of a gridded landuse map derived
591 from OpenStreetMap (© OpenStreetMap contributors 2020. Distributed under a Creative
592 Commons BY-SA License).
593



594
595
596
597
598
599

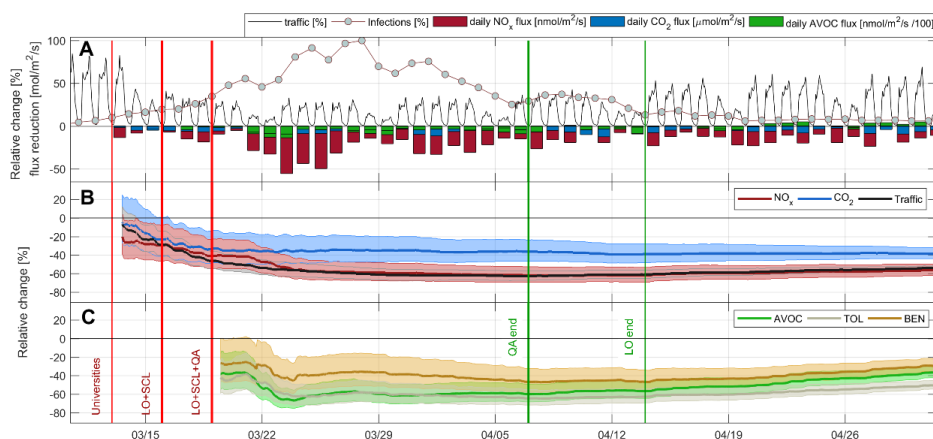
Fig. 2 (A): Time series of ambient NO₂ and NO_x mixing ratios before and during the lockdown. Shaded gray vertical bars indicate weekends. The gray vertical solid line depicts the start of lockdown measures on March 16th 2020; **(B):** NO₂ vs NO_x during weekdays (Tuesday to Thursday); **(C):** NO₂ vs NO_x on Sundays



600
601 **Fig. 3** Diurnal variations of CO₂ (A) and NO_x (B) fluxes since 2018.
602



603



604

605

Fig. 4. Observed changes of air pollutant fluxes, CO₂ flux and traffic during the course of the first SARS-CoV2 wave: **(A)** Normalized traffic counts, daily infection rate and daily average flux reduction. **(B)** Cumulative reduction of NO_x, and CO₂ fluxes and traffic activity. **(C)** Cumulative reduction of aromatic VOCs (AVOC), toluene (TOL) and benzene (BEN) fluxes. Red vertical lines indicate the start of University closure, Austrian Lockdown (LO), school closure (SCL) and quarantine (QA) in the state of Tyrol. Green vertical lines show the lifting of mobility restrictions. Light shaded areas represent the uncertainty of the boosted regression tree model analysis (SI).

609

610

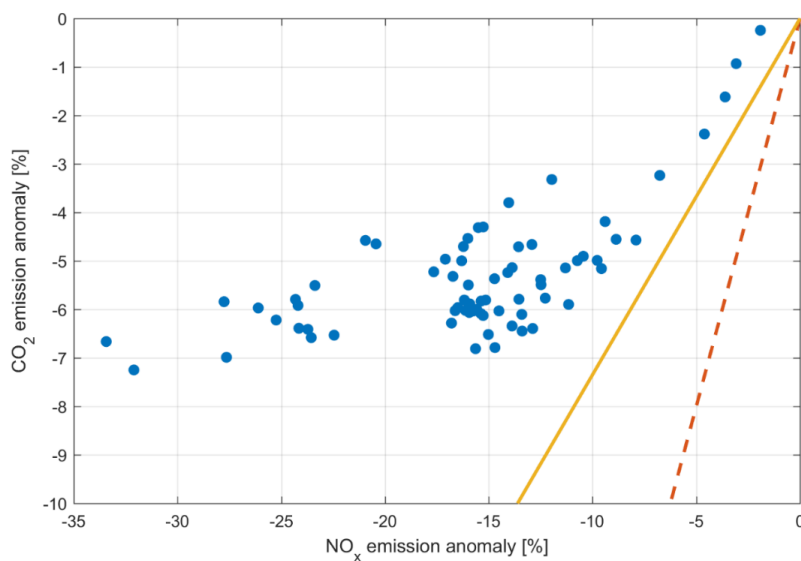
611

612

613



614



615
616
617
618
619

Fig. 5. Daily change of CO₂ and NO_x fluxes during the lockdown period. Flux observations are depicted by the blue dots. Emission model projections are represented by the solid orange line (Austrian emission inventory) and the dashed red line (Quéré et al., 2020).